IET Generation, Transmission & Distribution

*Special Issue: Optimal Utilisation of Storage Systems in Transmission and Distribution Systems*

IET Journals
The Institution of Engineering and Technology

# Fault current limiter-battery energy storage system for the doubly-fed induction generator: analysis and experimental verification

ISSN 1751-8687
Received on 5th December 2014
Revised on 16th June 2015
Accepted on 26th June 2015
doi: 10.1049/iet-gtd.2014.1158
www.ietdl.org

*Wenyong Guo* ✉, *Liye Xiao*, *Shaotao Dai*

*Institute of Electrical Engineering, Chinese Academy of Sciences, Beijing 100190, People's Republic of China*
✉ *E-mail: wyguo@mail.iee.ac.cn*

**Abstract:** Weak low voltage ride-through (LVRT) ability and unstable output power are two major problems faced by the doubly-fed induction generator (DFIG). To solve these two problems simultaneously, a commercially available fault current limiter-battery energy storage system (FCL–BESS), which is suitable to be applied in a microgrid, is proposed in this study. During normal operation, the FCL–BESS stabilises the output power of DFIG by compensating the fluctuating component of DFIG output power with energy buffering capability provided by the battery energy storage system (BESS). On occurrence of a grid fault, the FCL–BESS enhances the LVRT ability of DFIG by inserting the fault current limiting inductor into the stator, which weakens the rotor back electromagnetic force voltage and limits the rotor overcurrent. The FCL–BESS also stabilises the DC-link voltage by the BESS, which further strengthens the controllability of grid-side converter and rotor-side converter. Moreover, the FCL–BESS is able to help grid voltage recover fast and smoothly by providing power support to the grid. Experiments under different conditions have been carried out with a 2 kW prototype to evaluate the performance of the proposed FCL–BESS. Experimental results show that the FCL–BESS have much better performance than using single fault current limiter or BESS and can solve the two problems faced by the DFIG simultaneously and effectively.

## 1 Introduction

The doubly-fed induction generator (DFIG) has the good merits of small size, low cost and light weight, which makes it popular in wind energy conversion market [1]. The DFIG, however, has two major problems to overcome.

The first one is that it has weak low voltage ride through (LVRT) capability. The direct connection of the stator to the grid has made DFIG very sensitive to grid disturbance. An abrupt change in the grid voltage results in DC and negative sequence stator flux, which induces high rotor back electromagnetic force (EMF) voltage. The induced rotor back EMF voltage exceeds the voltage control range of rotor-side converter (RSC), which results in overcurrent of RSC and overtorque of gear box. The wind energy conversion system (WECS) of DFIG may therefore be destroyed. To solve this problem, many solutions have been proposed and can generally be classified into hardware [2–11] and software solutions [12–20].

The crowbar circuit [2, 3] is the most popular hardware solution to solve this problem. The crowbar is activated and the RSC is blocked as soon as rotor overcurrent is detected. The RSC is thus isolated from the rotor and prevented from overcurrent. However, the DFIG is changed into a squirrel cage induction machine and absorbs reactive power from the grid, which is not allowed by the grid connection requirement [1]. DC-link protection schemes, such as DC-link chopper [4] and energy storage system [5, 6] connected to the DC link are suggested to be used to protect the DC link from overvoltage. The series converters like series grid-side converters (GSCs) [7] and dynamic voltage restorers [8] are proposed to avoid abrupt changes of the stator voltage. The DFIG is therefore isolated from the grid fault to some extent. Additional resistance circuits [9–11] are also proposed to improve the LVRT performance of DFIG, which improves the damping performance of stator flux transient, limits rotor overcurrent, and weaken electromagnetic (EM) overtorque.

The software solutions: advanced control strategies have been proposed to enhance the LVRT capability of DFIG [12–21]. These control strategies can to some extent increase RSC control dynamics, limit rotor overcurrent, improve damping of DFIG transient response, minimise oscillations of EM torque, and provide better reactive power support to the grid. However, LVRT enhancing control strategies cannot provide fault ride through capability under severe grid fault conditions, since the RSC cannot supply the voltage as high as the rotor back EMF voltage because of DC-link voltage limitation [12, 13].

The second major problem faced by DFIG is the instable output power, which is due to the inherent property of wind and is the common problem faced by most WECSs. Below rated wind speed, almost all of the wind turbines are controlled to maximise active power output. The output power of the wind turbine therefore varies with wind speed. With the increasing penetration of wind power generation, the grid is subjected to voltage and frequency fluctuations. Although the wind turbine can be controlled to make less effort to maximize power output so as to smooth the energy production, much less energy will be generated. Moreover, it is not cost effective in the long run. To maximise and smooth the wind energy output simultaneously, energy storage is usually used [22–27].

To solve these two problems simultaneously, a superconducting fault current limiter-magnetic energy storage (SFCL–MES) system has been presented by Guo *et al.* [6]. Since the approach was proposed, new contribution considering the optimisation of superconducting coil (SC) [28] and new circuit configuration for DC microgrid application [29] were proposed by other authors. The SFCL–MES combines the fault current limiting and energy storage functions into one device by using single SC, which makes it able to enhance the LVRT capability and smooth output power of DFIG simultaneously. The SFCL–MES has the advantage of low annual cost because of high efficiency. However, the investment cost is still too high, which requires a long time to

recover the cost and makes is unable to realise commercialisation at present stage. Moreover, the effectiveness of the proposal was initially only validated by simulation studies. The roles of fault current limitation and energy storage in enhancing the LVRT capability of DFIG have not been clarified, and the interaction between current limitation and LVRT enhancing control has not been investigated.

As a subsequent contribution to [6], one major contribution of this paper is to present a much more commercially feasible way: a fault current limiter-battery energy storage system (FCL–BESS) to solve the two problems.

The topology of the FCL–BESS consists of two parts: the fault current limiter (FCL) part and the battery energy storage system (BESS) part. The FCL part is mainly used to enhance the LVRT capability of DFIG. The cost of the FCL part is higher than the conventional LVRT enhancing circuit: the crowbar circuit. However, the LVRT performance of the FCL part is much higher than the crowbar circuit since it avoids adsorbing reactive power from the grid, which is not allowed by the new grid code. The BESS part is used to smooth the active power output of DFIG and further enhance the LVRT capability of DFIG by stabilising the DC-link voltage. The cost of the BESS part is lower than the installation of an independent BESS, since the BESS part is integrated into the energy conversion system of DFIG and additional inverter circuit is avoided to be used. By integrating both FCL part and BESS part into the energy conversion system of DFIG, the performances of DFIG under both normal and grid fault conditions are greatly improved, which make it cost effective in certain applications.

Compared with FCL–BESS, the advantage of SFCL–MES is that it is simple in electrical topology by utilising the SC as the energy storage device and fault current limiting inductor simultaneously. However, additional equipments, such as cryostat and cryocooler are needed to maintain cryogenic environment. Considering the expensive superconductor and cryocooler, the investment cost of SFCL–MES is currently unacceptable for commercial application. The FCL–BESS is relatively complex in electrical topology. However, no additional equipments are needed, which makes it simple in maintenance. Moreover, all of the elements used in FCL–BESS are commercially available, which makes it easier to be applied at current stage.

The application field of FCL–BESS is mainly in the microgrid where the output power of one DFIG accounts for a large proportion of the microgrid. The oscillating output power of one DFIG will cause significant voltage and frequency fluctuations of the microgird. Moreover, the LVRT capability of one DFIG significantly influences the stability of the microgrid during the grid fault.

Another major contribution of this paper is to clarify and verify the roles of fault current limiting and energy storage functions in enhancing the LVRT capability of DFIG through extensive experimental evaluations. A 2 kW rated prototype has been set up. Experiments without hardware protection, with only BESS, with only FCL, and with FCL–BESS under both symmetrical and asymmetrical fault conditions have been carried out. Experimental results show that the fault current limiting function provides the major LVRT enhancing capability, while the energy storage function further strengthens the controllability of DFIG and smooth the fault recovery process. The FCL–BESS combines the fault current limiting and energy storage function into one device with commercially available materials and components, which makes it able to provide a comprehensive and promising solution to solve almost all of the DFIG related problems.

This paper is organised as follows: the model of DFIG under LVRT is presented in Section 2; the operational principles are illustrated in Section 3; control design is presented in Section 4; experimental results are presented in Section 5 to help evaluate the performance of the FCL–BESS; conclusions are drawn in Section 6.

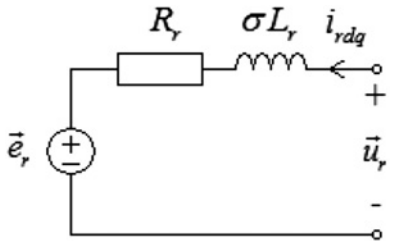


**Fig. 1** *Equivalent circuit from rotor side*

## 2 Model of DFIG under LVRT

The model of the DFIG in the stationary frame can be expressed as

$$\boldsymbol{u}_{\mathrm{s}} = R_{\mathrm{s}}\boldsymbol{i}_{\mathrm{s}} + \frac{\mathrm{d}}{\mathrm{d}t}\boldsymbol{\psi}_{\mathrm{s}} \tag{1}$$

$$\boldsymbol{u}_{\mathrm{r}} = R_{\mathrm{r}}\boldsymbol{i}_{\mathrm{r}} + \frac{\mathrm{d}}{\mathrm{d}t}\boldsymbol{\psi}_{\mathrm{r}} \tag{2}$$

$$\boldsymbol{\psi}_{\mathrm{s}} = L_{\mathrm{s}}\boldsymbol{i}_{\mathrm{s}} + L_{\mathrm{m}}\boldsymbol{i}_{\mathrm{r}} \tag{3}$$

$$\boldsymbol{\psi}_{\mathrm{r}} = L_{\mathrm{m}}\boldsymbol{i}_{\mathrm{s}} + L_{\mathrm{r}}\boldsymbol{i}_{\mathrm{r}} \tag{4}$$

$$L_{\mathrm{s}} = L_{\mathrm{ls}} + L_{\mathrm{m}} \tag{5}$$

$$L_{\mathrm{r}} = L_{\mathrm{lr}} + L_{\mathrm{m}} \tag{6}$$

$$T_e = \frac{3}{2}P\mathrm{Im}(\boldsymbol{i}_{\mathrm{s}}\boldsymbol{\psi}_{\mathrm{s}}^{*}) \tag{7}$$

where the $u$, $i$, $\psi$, $R$, and $L$ represent voltage, current, flux linkage, resistance, and inductance respectively. Subscripts s, r, l, and m denote the stator, rotor, leakage, and mutual quantities, respectively, and $P$ is the number of pole pairs.

From (2)–(4), the rotor voltage can be expressed as

$$\boldsymbol{u}_{\mathrm{r}} = \frac{L_{\mathrm{m}}}{L_{\mathrm{s}}}\frac{\mathrm{d}}{\mathrm{d}t}\boldsymbol{\psi}_{\mathrm{s}} + \left(R_{\mathrm{r}} + \sigma L_{\mathrm{r}}\frac{\mathrm{d}}{\mathrm{d}t}\right)\boldsymbol{i}_{\mathrm{r}} \tag{8}$$

where $\sigma = 1 - (L_{\mathrm{m}}^2/L_{\mathrm{s}}L_{\mathrm{r}})$ is the leakage coefficient.

The first term is the rotor back-EMF voltage and defined as $\boldsymbol{e}_{\mathrm{r}}$. The second term is the voltage drop on the rotor resistance and rotor transient inductance $\sigma L_{\mathrm{r}}$. The equivalent circuit is shown in Fig. 1.

The stator voltage can be expressed as

$$\boldsymbol{u}_{\mathrm{s}} = V_{\mathrm{s}}^{\mathrm{p}}\,\mathrm{e}^{\mathrm{j}\omega_{\mathrm{s}}t} + V_{\mathrm{s}}^{\mathrm{n}}\,\mathrm{e}^{-\mathrm{j}\omega_{\mathrm{s}}t} + V_{\mathrm{s}}^{0} \tag{9}$$

where $\omega$ represents the angular frequency. The superscripts p, n, and 0 denote positive, negative, and zero sequence quantities, respectively.

Since the zero sequence voltage does not create flux [1], the stator flux induced by stator voltage can be expressed as

$$\boldsymbol{\psi}_{\mathrm{s}} = \frac{V_{\mathrm{s}}^{\mathrm{p}}}{\mathrm{j}\omega_{\mathrm{s}}}\mathrm{e}^{\mathrm{j}\omega_{\mathrm{s}}t} + \frac{V_{\mathrm{s}}^{\mathrm{n}}}{-\mathrm{j}\omega_{\mathrm{s}}}\mathrm{e}^{-\mathrm{j}\omega_{\mathrm{s}}t} + \psi_{\mathrm{n0}}\,\mathrm{e}^{-t/\tau_{\mathrm{s}}} \tag{10}$$

where $\psi_{\mathrm{n0}}$ is the initial value of natural flux, $\tau_{\mathrm{s}} = L_{\mathrm{s}}/R_{\mathrm{s}}$ is the time constant of stator flux linkage, $V_{\mathrm{s}}^{\mathrm{p}}$ and $V_{\mathrm{s}}^{\mathrm{n}}$ are the magnitudes of stator positive and negative sequence voltages after the fault. $\psi_{\mathrm{n0}}$ is the initial natural flux, which is decided by the angle $\varphi_{\psi 0}$ between positive and negative sequence components of stator flux and has the largest value if $\varphi_{\psi 0} = \pi$ [12].

Transferring (9) into reference frame fixed on the rotor, we have

$$\boldsymbol{\psi}_{\mathrm{s}} = \frac{V_{\mathrm{s}}^{\mathrm{p}}}{\mathrm{j}\omega_{\mathrm{s}}}\mathrm{e}^{\mathrm{j}(\omega_{\mathrm{s}}-\omega_{\mathrm{r}})t} + \frac{V_{\mathrm{s}}^{\mathrm{n}}}{-\mathrm{j}\omega_{\mathrm{s}}}\mathrm{e}^{-\mathrm{j}(\omega_{\mathrm{s}}+\omega_{\mathrm{r}})t} + \psi_{\mathrm{n0}}\,\mathrm{e}^{-t/\tau_{\mathrm{s}}}\,\mathrm{e}^{-\mathrm{j}\omega_{\mathrm{r}}t} \tag{11}$$


*IET Gener. Transm. Distrib.*, 2016, Vol. 10, Iss. 3, pp. 653–660

From (10), the rotor back-EMF voltage can be represented as

$$\boldsymbol{e}_{\mathrm{r}}=\frac{L_{\mathrm{m}}}{L_{\mathrm{s}}}\left[s\boldsymbol{V}_{\mathrm{s}}^{\mathrm{p}}\,\mathrm{e}^{\mathrm{j}s\omega_{\mathrm{s}}t}+(2-s)\boldsymbol{V}_{\mathrm{s}}^{\mathrm{n}}\,\mathrm{e}^{-\mathrm{j}(2-s)\omega_{\mathrm{s}}t}-\left(\frac{1}{\tau_{\mathrm{s}}}+\mathrm{j}\omega_{\mathrm{r}}\right)\psi_{\mathrm{n0}}\,\mathrm{e}^{-((1/\tau_{\mathrm{s}})+\mathrm{j}\omega_{\mathrm{r}})t}\right] \tag{12}$$

Since time constant of the stator flux is relative large, $(1/\tau_{\mathrm{s}})$ can be neglected, (12) can be simplified as

$$\boldsymbol{e}_{\mathrm{r}}=\frac{L_{\mathrm{m}}}{L_{\mathrm{s}}}\left[s\boldsymbol{V}_{\mathrm{s}}^{\mathrm{p}}\,\mathrm{e}^{\mathrm{j}s\omega_{\mathrm{s}}t}+(2-s)\boldsymbol{V}_{\mathrm{s}}^{\mathrm{n}}\,\mathrm{e}^{-\mathrm{j}(2-s)\omega_{\mathrm{s}}t}-\mathrm{j}\omega_{\mathrm{r}}\psi_{\mathrm{n0}}\,\mathrm{e}^{-((1/\tau_{\mathrm{s}})+\mathrm{j}\omega_{\mathrm{r}})t}\right] \tag{13}$$

## 3 Operational principle

### 3.1 Topology of the FCL–BESS

The topology of the FCL–BESS is shown in Fig. 2. The FCL part consists of three coupling transformers, a diode bridge, a fault current limiting inductor (FCLI, Lt), and a current source chopper (CSC). The BESS part consists of an LC (Le and Ce) filter, a battery pack (Be), and a voltage source chopper (VSC). The CSC and VSC share the same DC link with the GSC and RSC of the DFIG.

### 3.2 Operational principle under normal operation

Under normal operation, the FCL must have minimal effect on the proper operation of the DFIG. To reach this objective, the CSC is controlled to regulate the FCLI current to a constant value ($I_{\mathrm{FCLI}}^{*}$), which is higher than $n$ ($n$ is the transformer turn ratio) times that of the maximum possible peak stator current. The diode bridge is thus fully conducting. The stator current freewheels through the diodes. The on-state voltage drops of diodes and the voltage drops of the winding resistance and the leakage inductance are the only voltage drops on the FCL, which is negligibly small compared to the stator voltage of the DFIG. The proper operation of the DFIG is therefore unaffected by the series connected FCL.

The GSC is controlled to fulfil the active power fluctuation compensation function. To reach this objective, a low-pass filter (LPF) is used to extract the stator output average active power. The difference between the stator output average and instantaneous active power is the reference active power command of the GSC. The BESS is used to control the DC-link voltage to a constant reference value. If the GSC absorbs active power from the grid, the DC-link voltage tends to rise. By regulating the DC-link voltage, the BESS transfers the excess energy stored in the DC-link capacitor to the battery and causes the DC-link voltage to decrease towards the reference value. The BESS thus transfers the GSC absorbed active power to the battery indirectly. On the contrary, if the GSC output active power to the grid, the BESS will transfer the energy stored in the battery to the grid indirectly in the similar way. The way that the DC-link voltage is controlled by the BESS is more advantageous than that controlled by the GSC [25]. This is because that the GSC cannot output enough active power to stabilise the DC-link voltage when the grid voltage drops to a very low value. Whereas, the active power output capability of BESS is uninfluenced by the grid voltage, which make the DC-link voltage able to be kept in the controllable state even under severe grid fault conditions. The LVRT capability is therefore better enhanced with the better controlled DC-link voltage.

### 3.3 Operational principle under grid fault

On occurrence of a grid fault, the stator current increases in amplitude and reaches the threshold ($I_{\mathrm{FCLI}}^{*}/n$). The diode strings become reverse biased, and the FCLI is automatically switched into the stator circuits and limits the stator overcurrent. After the grid fault is cleared, the stator current decreases in amplitude. When the stator current amplitude is lower than the threshold value, the blocked diodes regain forward conducting and the FCLI is disconnected from the stator circuit automatically. Since the induction machine can be regarded as a rotating transformer, the rotor overcurrent can also be limited by magnetic coupling.

The interaction between fault current limitation and LVRT is explained as follows:

The first interaction effect is that the fault current limitation has weakened rotor back-EMF voltage, which enhances the controllability of RSC so that the LVRT capability is improved.

The rotor back-EMF voltage after insertion of FCLI is changed from (13) to

$$\boldsymbol{e}_{\mathrm{r}}^{\prime}=\frac{L_{\mathrm{m}}}{L_{\mathrm{s}}+n^{2}L_{\mathrm{l}}}\left[s\boldsymbol{V}_{\mathrm{s}}^{\mathrm{p}}\,\mathrm{e}^{\mathrm{j}s\omega_{\mathrm{s}}t}+(2-s)\boldsymbol{V}_{\mathrm{s}}^{\mathrm{n}}\,\mathrm{e}^{-\mathrm{j}(2-s)\omega_{\mathrm{s}}t}-\mathrm{j}\omega_{\mathrm{r}}\psi_{\mathrm{n0}}\,\mathrm{e}^{-((1/\tau_{\mathrm{s}}^{\prime})+\mathrm{j}\omega_{\mathrm{r}})t}\right] \tag{14}$$

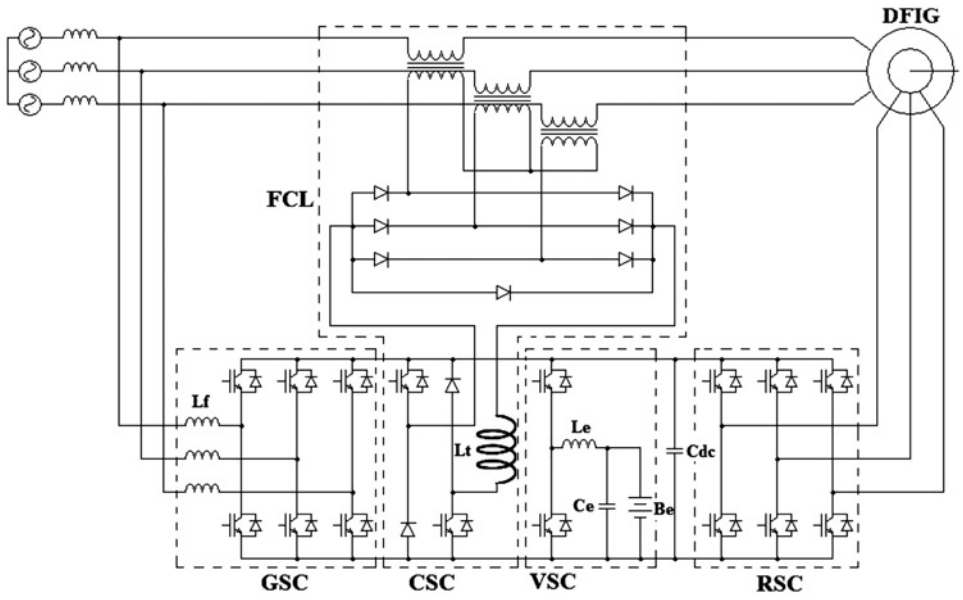


**Fig. 2** *Topology of the FCL–BESS incorporated in a DFIG*

where $\tau_s^e = (L_s + n^2L_l)/(R_s + n^2R_l)$, $L_l$ and $R_l$ are the inductance and resistance of the FCLI.

Upon insertion of FCLI, the denominator of (14) is increased from $L_s$ to $(L_s + n^2L_l)$. Since $(L_s + n^2L_l) > L_s$, the rotor back-EMF voltage can thus be weakened by the FCL, which increases the controllability of the RSC. The LVRT capability can therefore be enhanced.

The second interaction effect is that it increases the rotor transient inductance, which further prevents the RSC from overcurrent. The leakage coefficient after switching operation is changed to be

$$\sigma^e = 1 - \frac{L_m^2}{(L_s + n^2L_l)L_r} \tag{15}$$

Upon insertion of FCLI, the denominator of the second term in (15) is increased from $L_sL_r$ to $(L_s + n^2L_l)L_r$. Since the second term in (15) is decreased, the rotor transient inductance $\sigma^eL_r$ is increased. The rotor overcurrent can thus be limited with larger $\sigma^eL_r$. The RSC can therefore be protected from overcurrent.

## 4 Control design of the FCL–BESS

### 4.1 LVRT control strategy

LVRT control is implemented by the RSC. The control target is set to constrain the rotor overcurrent in a way that requires a minimum rotor voltage. From (2), the rotor voltage is mainly determined by the derivative of rotor flux. To keep the rotor voltage under controllable range, the rotor flux is controlled to make its derivative value kept within an acceptable range.

From (3) and (4), the rotor flux can be expressed as

$$\boldsymbol{\psi}_r = L_m/L_s \times \boldsymbol{\psi}_s + \sigma L_r \boldsymbol{i}_r \tag{16}$$

The derivative of the first term is $\boldsymbol{e}_r^r$, whose dominating terms are determined by the DC and negative sequence stator flux. To reduce the rotor overvoltage, $\boldsymbol{i}_r$ is controlled by the RSC to counteract the DC and negative sequence stator flux. To fully counteract the DC and negative sequence stator flux, the reference value of $\boldsymbol{i}_r$ can be selected as [11]

$$\boldsymbol{i}_r^* = -\frac{L_m}{\sigma L_r L_s}\boldsymbol{\psi}_s^{0,n} \tag{17}$$

where $\boldsymbol{\psi}_s^{0,n}$ is the sum of the DC and negative sequence stator flux.

After insertion of the FCLI, $\boldsymbol{i}_r^*$ is changed to be

$$\boldsymbol{i}_r^* = -\frac{L_m}{\sigma^e L_r (L_s + n^2L_l)}\boldsymbol{\psi}_s^{0,n} \tag{18}$$

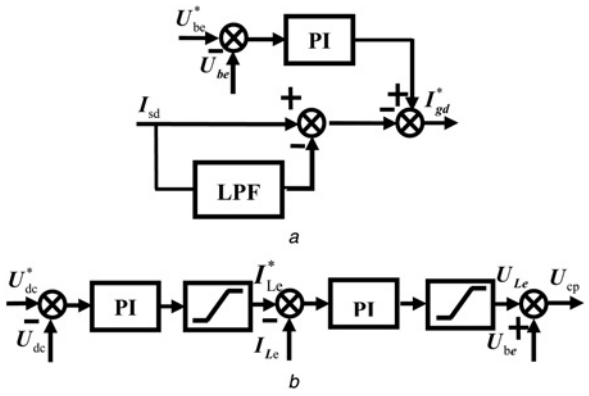


**Fig. 3** *Control block diagram*
*a* Active current control of GSC
*b* Control of BESS

As can be seen from (18), the denominator is increased compared with that of (17). This is due to the increase of rotor transient inductance $\sigma^eL_r$ and equivalent stator inductance $(L_s + n^2L_l)$. The magnitude of $\boldsymbol{i}_r^*$ can therefore be decreased with the help of FCL, which decreases current rating requirement of RSC. This also means that the FCL can not only weaken the rotor back-EMF voltage, limits rotor overcurrent, but also strengthen the LVRT enhancing controllability of RSC. With the cooperation of FCL and LVRT enhancing control, the LVRT capability of the DFIG can be greatly strengthened.

### 4.2 Active power fluctuation compensation control strategy

Active power fluctuation compensation is realised by the GSC. The *dq* components of the stator current represent the stator active and reactive currents. To compensate the stator active power fluctuations, a LPF is used to extract the fluctuating component of active current. The GSC is also used to regulate the battery voltage to a balanced value so as make it not to deviate from normal operational range in the long run, which is realised by a proportion–integral (PI) regulator. The input of the PI regulator is the reference and measured battery voltages ($U_{be}^*$ and $U_{be}$), respectively. The corresponding active current control block diagram is shown in Fig. 3*a*.

### 4.3 BESS control strategy

The BESS is controlled to stabilise the DC-link voltage, which indirectly supplies energy to fulfil the active power smoothing function. The battery output voltage and current have to be constrained within an acceptable range to protect the battery from overvoltage and overcurrent. A double-loop control strategy is therefore used to both stabilise DC-link voltage and protect the battery. The outer loop is a voltage control loop. The input of the outer loop is the error between reference and measured DC-link voltages ($U_{dc}^*$ and $U_{dc}$). To protect the battery from overcurrent, the output of the outer loop is limited to be within an acceptable range and set as the reference current of filter inductor ($L_e$). The inner control loop is a current control loop. The input of the inner loop is the error between the reference and measured $L_e$ currents ($I_{L_e}^*$ and $I_{L_e}$), the output of the inner loop is the voltage across $L_e(U_{L_e})$. To protect the battery from overvoltage, the output of the inner loop is also limited to be within an acceptable range. The output command voltage of the VSC ($U_{cp}$) is the sum of $U_{L_e}$ and $U_{be}$. The control diagram is shown in Fig. 3*b*.

## 5 Experimental evaluation

Experiments are carried out to evaluate the performance of the FCL–BESS. Experimental setup is shown in Fig. 4. Three 3 mH air-core inductors are used to simulate the source impedance. A vacuum contactor is connected right after the air-core inductors to generate voltage sags with depths up to 100%. The DFIG is driven by a motor, which is driven by a converter.

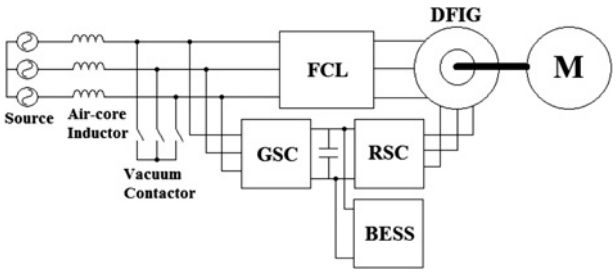


**Fig. 4** *Experimental setup*


*IET Gener. Transm. Distrib.*, 2016, Vol. 10, Iss. 3, pp. 653–660

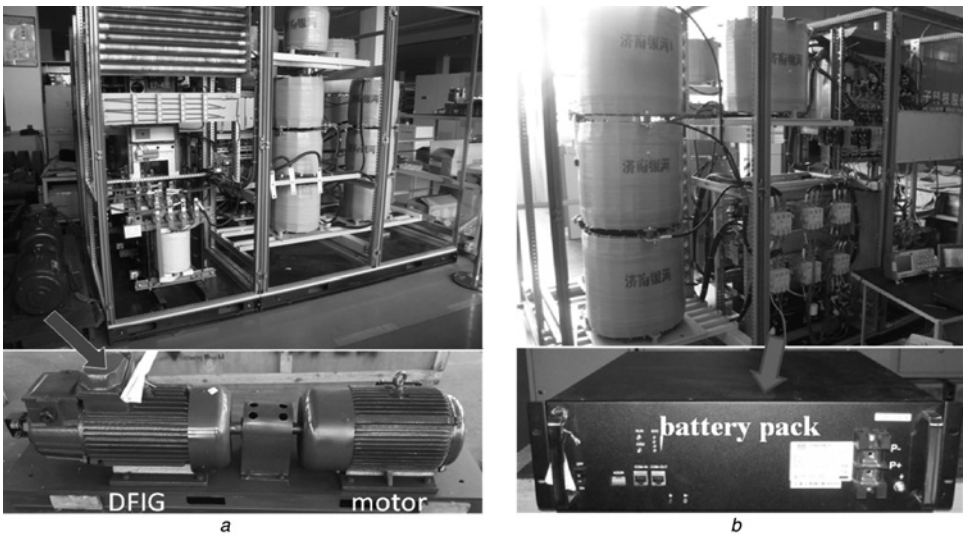


**Fig. 5** *Experimental platform*

*a* Front view
*b* Rear view

An experimental platform is shown in Fig. 5. The experimental parameters are listed in Tables 1 and 2. During normal operation, the motor is driven at a variable speed. The output power of DFIG varies with the varying shaft speed.

### 5.1 Active power fluctuation compensation result

Fig. 6 shows the active power fluctuation compensation result. All quantities of experimental results are computed by the digital signal processor (DSP) of DFIG and output by the digital-to-analogue output ports of DSP control board. From top to bottom, the lines in the figure are the output active power of DFIG, the whole system, and BESS, respectively.

From Fig. 6, it can be found out that the DFIG output power fluctuates significantly with varying shaft speed. The output power of the whole system, however, remains almost constant. The BESS outputs oscillating terms of the DFIG output active power with opposite sign to realise active power fluctuation compensation. The output power of the DFIG is thus effectively smoothed and has little adverse impact on the grid.

### 5.2 LVRT results under symmetrical fault

Fig. 7 shows the experimental results under symmetrical fault condition. A three-phase short-circuit fault happens at the terminal of the stator. The grid voltage drops to zeroes during the grid fault. Figs. 7*a–d* show the experimental results without hardware protection, with only BESS, with only FCL, and with FCL–BESS, respectively. In all of the four experiments, the RSC uses the same LVRT control strategy as illustrated in Section 4. From top to bottom, the four lines in the figures represents the positive sequence grid voltage magnitude estimated by Kalman filter [30], DC-link voltage, rotor current magnitude, and EM torque, respectively.

Without hardware protection, significant overcurrent and overtorque can be found out in Fig. 7*a*. Rotor overcurrent reaches to be more than two times that of the nominal value, and EM overtorque reaches to be more than four times that of the nominal value. The DC-link voltage also loses control during this process. This is because the grid voltage drops to zero and the GSC cannot supply active power to stabilise the DC-link voltage. The grid voltage also fluctuates severely upon recovery of the grid fault, which is because the DFIG is out of control and cannot provide proper power support to the grid with the unstable DC-link voltage.

From Fig. 7*b*, it can be found out that overcurrent and overtorque are not alleviated with the BESS. Similar overcurrent and overtorque magnitudes as that of the previous case can be observed. However, the DC-link voltage remains almost constant during the grid fault. This is because the DC-link voltage is controlled by the BESS. The active power control capability of the BESS is not influenced by the grid fault, and the BESS is still able to control the DC-link voltage during the grid fault. The grid voltage also recovers much fast and smoothly upon recovery of the grid fault. This is because the stabilised DC-link voltage strengthens the controllability of GSC and RSC, which makes it able to provide proper power support to the grid.

From Fig. 7*c*, it can be found out that overcurrent and overtorque are greatly alleviated with the FCL. The rotor overcurrent and EM overtorque are kept within 1.2 and 1.5 times that of their nominal values upon occurrence of a grid fault. The RSC and gearbox can thus be protected. Since the grid voltage drops to zero, the GSC cannot provide active power support to the DC link. Furthermore, the DC-link voltage is under controllable state and fluctuates severely upon and during recovery of the grid fault. The grid voltage recovers slowly after the grid fault, which is because the DFIG cannot provide proper power support to the grid with the unstable DC-link voltage.

**Table 1** 2 kW DFIG experimental parameters

| Symbol | Quantity | Value |
|---|---|---|
| $L_m$ | magnetising inductance | 72.4 mH |
| $L_{ls}$, $L_l$ | stator and rotor leakage inductances | 2.15 mH, 4.1 mH |
| $R_s$, $R_r$ | stator and rotor resistances | 0.689 Ω, 0.55 Ω |
| $P$ | number of pole pairs | 3 |
| $N_{rs}$ | rotor-to-stator turns ratio | 3 |

**Table 2** FCL–BESS experimental parameters

| Symbol | Quantity | Value |
|---|---|---|
| $L_l$, $R_l$ | inductance and resistance of fault current limiting inductor | 9 mH, 0.1 Ω |
| $n$ | transformer turn ratio | 2:1 |
| $U_{be}$ | battery rated voltage | 96 V |
| $E_{be}$ | battery capability | 50 Ah |
| $L_e$ | battery chopper filter inductance | 10 mH |
| $C_e$ | battery chopper filter capacitance | 6.6 mF |

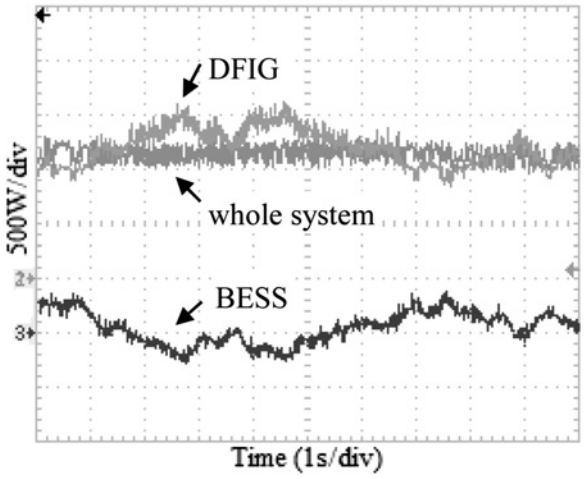


**Fig. 6** *Active power fluctuation compensation result*

From Fig. 7*d*, it can be also found out that the overcurrent and overtorque are effectively limited with the FCL–BESS as that of the FCL case. The grid voltage recovers fast and smoothly with stabilised DC-link voltage and power smoothing capability provided by the BESS. The FCL–BESS is thus able to provide the best LVRT performance among the four cases.

### 5.3 LVRT results under asymmetrical fault

Fig. 8 shows the experimental result under asymmetrical fault condition. The grid fault is the phase-to-phase short-circuit fault, which is considered to be the worst condition [13]. Figs. 8*a*–*d* show the experimental results without protection, with only BESS, with only FCL, and with FCL–BESS, respectively.

From Fig. 8*a*, it can be found out that the overcurrent and overtorque are even more severe than that of the symmetrical fault case. The overcurrent and overtorque magnitudes reach to be about three and five times that of the nominal value. This is due to the impact of the negative sequence grid voltage, which increases the rotor back-EMF voltage. The DC-link voltage, unlike the symmetrical fault case, remains nearly constant, which is due to that the GSC, can still provide active power support to the DC-link voltage under asymmetrical fault.

From Figs. 8*c* and *d*, overcurrent and overtorque have been limited within 1.5 and 2 times that of the nominal values with FCL and FCL–BESS. Compared with Figs. 8*a* and *b*, the advantage of using BESS is smoother recovery of grid voltage. Compared with Figs. 8*a* and *c*, the advantage of using FCL is better limitation of overcurrent and overtorque, which helps to protect the RSC and gearbox. Compared with Figs. 8*a* and *d*, the FCL–BESS not only limits overcurrent and overtorque, but also helps the grid voltage recover smoothly, which is coincident with the previous symmetrical case.

### 5.4 Experimental result discussion

As can be seen from the experimental results, both the FCL and BESS have impacts on the LVRT of DFIG. From Figs. 7*c* and 8*c*, overcurrent and overtorque are sufficiently limited with only FCL, which demonstrates that the current limiting function plays the dominant role in the LVRT capability enhancement. The FCL limits the stator overcurrent so that the rotor overcurrent is also limited by magnetic coupling. From (7), the EM torque is proportional to the stator current, the EM overtorque is therefore

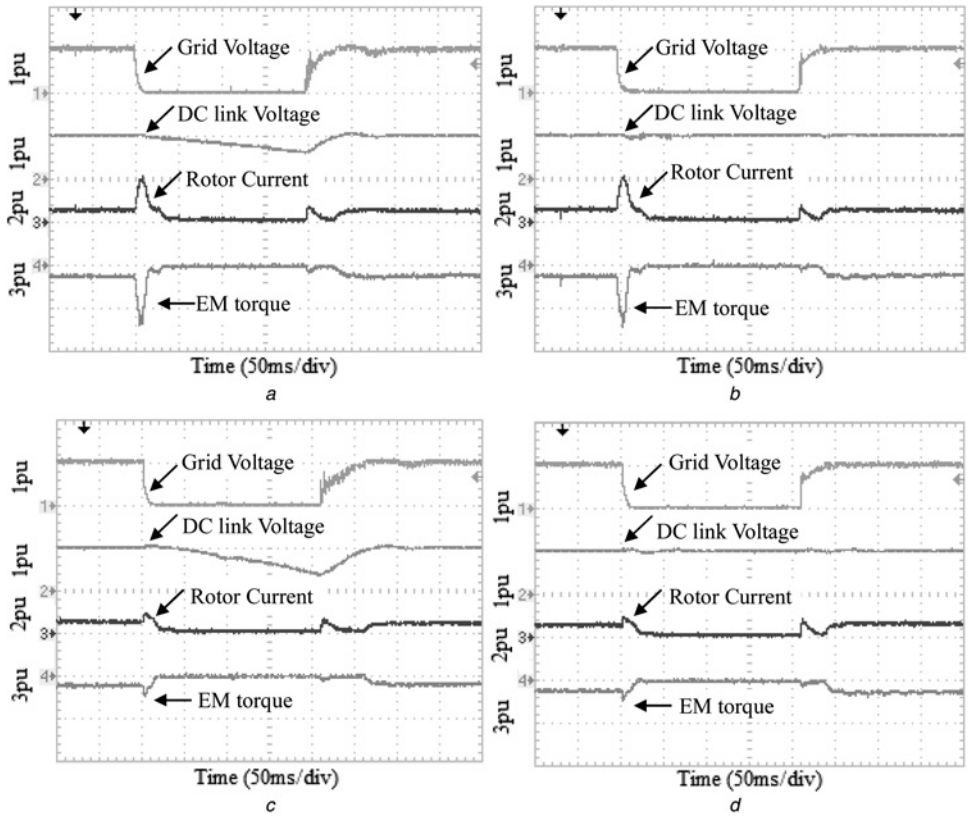


**Fig. 7** *Experimental results under symmetrical fault*

*a* Without hardware protection
*b* With only BESS
*c* With only FCL
*d* With FCL–BESS


*IET Gener. Transm. Distrib.*, 2016, Vol. 10, Iss. 3, pp. 653–660

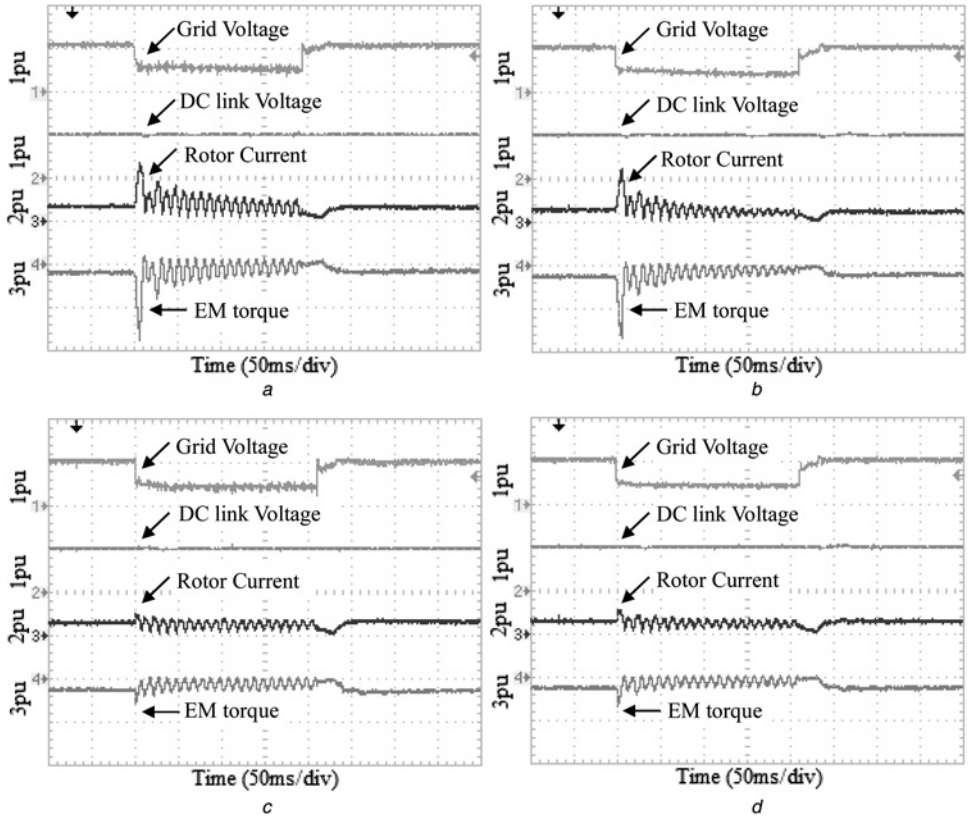


**Fig. 8** *Experimental results under asymmetrical fault*

*a* Without hardware protection
*b* With only BESS
*c* With only FCL
*d* With FCL–BESS

effectively limited with the limited stator overcurrent. The BESS plays auxiliary LVRT role by preventing DC-link voltage from overvoltage. The active power capability of BESS is unaffected by the grid voltage sag, which makes it able to provide DC-link stabilising capability superior to that of the GSC. The interaction between the FCL and BESS can be found between Figs. 8*c* and *d*. By preventing DC-link voltage from overvoltage with the BESS, the output voltage capability of the RSC is weakened with lower DC-link voltage. The overcurrent and overtorque limiting performance of the FCL–BESS, although still acceptable, is therefore slightly worse than that of the FCL.

## 6 Conclusion

This paper presents an FCL–BESS to both smooth the active power output and enhance the LVRT capability of DFIG. The operational principle of the proposed FCL–BESS is presented. An experimental platform has been set up to evaluate both active power smoothing and LVRT enhancing performances. Experiments under four different conditions (without hardware protection, with only BESS, with only FCL and with FCL–BESS) are carried out to evaluate the contributions of FCL and the BESS to the LVRT performance of DFIG. Since the same LVRT control strategy is used in all of the cases, the different LVRT performances in these cases are mainly due to the different circuit configurations. The following conclusions can be drawn based on the analysis and experimental results.

(i) The fault current limiting function of the FCL–BESS can limit DFIG overcurrent and overtorque during LVRT, which is the main reason that the FCL–BESS can enhance the LVRT capability of DFIG.

(ii) The FCL can further strengthen the LVRT enhancing control performance by weakening the rotor back-EMF voltage and increasing rotor transient inductance.

(iii) The energy storage function of the FCL–BESS can smooth the active output power fluctuations of DFIG during normal operation with the energy buffering capability provided by the BESS.

(iv) The energy storage function of the FCL–BESS can stabilise the DC-link voltage of DFIG and help the grid voltage recover smoothly by providing power support to the grid, which further improves the LVRT capability of DFIG.

(v) The combination of the fault current limiting and energy storage functions shows the great advantage over single function and is seemly a promising solution to solve almost all of the DFIG related problems.

## 7 Acknowledgments

This work was supported in part by the National Natural Science Foundation of China (NSFC) under Grant 50907070, 51361135705 and in part by National High-tech R&D Program of China (863 Program) under Grant 2013AA050803.

## 8 References

1 Cardenas, R., Pena, R., Alepuz, S., Asher, G.: 'Overview of control system for the operation of DFIGs in wind energy application', *IEEE Trans. Ind. Electron.*, 2013, **60**, (7), pp. 2776–2798
2 Tohidi, S., Oraee, H., Zolghadri, M.R., Shao, S., Tavner, P.: 'Analysis and enhancement of low-voltage-ride-through capability of brushless doubly fed induction generator', *IEEE Trans. Ind. Electron.*, 2013, **60**, (3), pp. 1146–1155
3 Vidal, J., Abad, G., Arza, J., Aurtenechea, S.: 'Single-phase DC crowbar topologies for low voltage ride through fulfillment of high-power doubly fed induction generator-based wind turbines', *IEEE Trans. Energy Convers.*, 2013, **28**, (3), pp. 768–781

4 Pannell, G., Zahawi, B., Atkinson, D.J., Missailidis, P.: 'Evaluation of the performance of a DC-link brake chopper as a DFIG low-voltage fault-ride-through device', *IEEE Trans. Energy Convers.*, 2013, **28**, (3), pp. 535–542
5 Abbey, C., Joos, G.: 'Supercapacitor energy storage for wind energy applications', *IEEE Trans. Ind. Appl.*, 2007, **43**, (3), pp. 763–776
6 Guo, W., Xiao, L., Dai, S.: 'Enhancing low-voltage ride-through capability and smoothing output power of DFIG with a superconducting fault-current limiter–magnetic energy storage system', *IEEE Trans. Energy Convers.*, 2012, **27**, (2), pp. 277–295
7 Huang, P., Moursi, M.S.E., Xiao, W., Kirtley, J.L.: 'Novel fault ride-through configuration and transient management scheme for doubly fed induction generator', *IEEE Trans. Energy Convers*, 2013, **28**, (1), pp. 86–94
8 Ramirez, D., Martinez, S., Platero, C.A., Blazquez, F., de Castro, R.M.: 'Low-voltage ride-through capability for wind generators based on dynamic voltage restorers', *IEEE Trans. Energy Convers*, 2011, **26**, (1), pp. 195–203
9 Yang, J., Flectcher, J.E., O'Reilly, J.: 'A series dynamic resistor based converter protection scheme for doubly fed induction generator during various fault condition', *IEEE Trans. Energy Convers*, 2010, **25**, (2), pp. 422–432
10 Yan, X., Venkataramanan, G., Wang, Y., Dong, Q., Zhang, B.: 'Grid-fault tolerant operation of DFIG wind turbine generator using a passive resistance network', *IEEE Trans. Power Electron.*, 2011, **26**, (10), pp. 2896–2905
11 Mohammadi, J., Afsharnia, S., Vaez-Zadeh, S.: 'Efficient fault-ride-through control strategy of DFIG-based wind turbines during the grid fault', *Energy Convers. Manag.*, 2014, **78**, pp. 88–95
12 Xiao, S., Yang, G., Zhou, H., Geng, H.: 'An LVRT control strategy based on flux linkage tracking for DFIG-based WECS', *IEEE Trans. Ind. Electron.*, 2013, **60**, (7), pp. 2820–2832
13 Geng, H., Liu, C., Yang, G.: 'LVRT capability of DFIG-based WECS under asymmetrical grid fault condition', *IEEE Trans. Ind. Electron.*, 2013, **60**, (7), pp. 2495–2509
14 Xiao, S., Yang, G., Zhou, H., Geng, H.: 'Analysis of the control limit for rotor-side converter of doubly fed induction generator-based wind energy conversion system under various voltage dips', *IET Renew. Power Gener.*, 2013, **7**, (1), pp. 71–81
15 Long, T., Shao, S., Malliband, P., Abdi, E., McMahon, R.A.: 'Crowbarless fault ride-though of the brushless doubly fed induction generator in a wind turbine under symmetrical voltage dips', *IEEE Trans. Ind. Electron.*, 2013, **60**, (7), pp. 2495–2509
16 Yang, L., Xu, Z., Ostergaard, J., Dong, Z.Y., Wong, K.P.: 'Advanced control strategy of DFIG wind turbines for power system fault ride through', *IEEE Trans. Power Syst.*, 2012, **27**, (2), pp. 713–722
17 Hossain, M.J., Saha, T.K., Mithulannanthan, N., Pota, H.R.: 'Control strategies for augmenting LVRT capability of DFIGs in interconnected power system', *IEEE Trans. Ind. Electron.*, 2013, **60**, (7), pp. 2495–2509
18 Xie, D., Xu, Z., Yang, L., Ostergaard, J., Xue, Y., Wong, K.P.: 'A comprehensive LVRT control strategies for DFIG wind turbines with enhanced reactive power support', *IEEE Trans. Power Syst.*, 2013, **28**, (3), pp. 3302–3310
19 Liang, J., Howard, D.F., Restrepo, J.A., Harley, R.G.: 'Feedforward transient compensation control for DFIG wind turbines during both balanced and unbalanced grid disturbances', *IEEE Trans. Ind. Appl.*, 2013, **49**, (3), pp. 1452–1462
20 Bu, S.Q., Du, W., Wang, H.F., Gao, S.: 'Power angle control of grid-connected doubly fed induction generator wind turbines for fault ride-through', *IET Renew. Power Gener.*, 2013, **7**, (1), pp. 18–27
21 da Costa, J.P., Pinheiro, H., Degner, T., Arnold, G.: 'Robust controller for DFIGs of grid-connected wind turbines', *IEEE Trans. Ind. Electron.*, 2011, **58**, (9), pp. 4023–4038
22 Jiang, Q., Gong, Y., Wang, H.: 'A battery energy storage system dual-layer control strategy for mitigating wind farm fluctuations', *IEEE Trans. Power Syst.*, 2013, **28**, (3), pp. 3263–3272
23 Cstillo, A., Gayme, D.F.: 'Grid-scale energy storage applications in renewable energy integration: a survey', *Energy Convers. Manag.*, 2014, **87**, pp. 885–894
24 Zhao, P., Wang, J., Dai, Y.: 'Capacity allocation of a hybrid energy storage system peak shaving at high wind power penetration level', *Renew. Energy*, 2015, **75**, pp. 541–549
25 Xu, G., Xu, L., Morrow, J.: 'Power oscillation damping using wind turbine with energy storage systems', *IET Renew. Power Gener.*, 2013, **7**, (5), pp. 449–457
26 Diaz-Gonzalez, F., Bianchi, F.D., Sumper, A., Gomis-Bellmunt, O.: 'Control of a flywheel energy storage system for power smoothing in wind power plant', *IEEE Trans. Energy Convers.*, 2014, **29**, (1), pp. 204–214
27 Islam, F., Al-Durra, A., Muyeen, S.M.: 'Smoothing of wind farm output by prediction and supervisory-control-united- based FESS', *IEEE Trans. Sustain. Energy*, 2013, **4**, (4), pp. 925–933
28 Karaipoom, T., Ngamroo, I.: 'Optimal superconducting coil integrated into DFIG wind turbine for fault ride through capability enhancement and output power fluctuation suppression', *IEEE Trans. Sustain. Energy*, 2015, **6**, (1), pp. 28–42
29 Ngamroo, I., Karaipoom, T.: 'Improving low-voltage ride-through performance and alleviating power fluctuations of DFIG wind turbine in DC microgrid by optimal SMES with fault current limiting function', *IEEE Trans. Appl. Supercond.*, 2014, **24**, (5), p. 5700805
30 Guo, W., Xiao, L., Dai, S.: 'Control and design of a current source UPQC with fault current limiting ability', *IET Power Electron.*, 2013, **6**, (2), pp. 297–308